Divergent Flow Effects in Cellular Detonations

Stephen Voelkel, Mark Short and Carlos Chiquete
Los Alamos National Laboratory
Los Alamos, NM, USA

1 Introduction

Continuous detonation engines maintain detonations in static geometries, achieving significant performance and efficiency [1]. A general flow schematic for this class of systems in a planar configuration is shown in Fig. 1. As the detonation passes through the geometry, fuel is pushed into the channel, replacing the detonation products and effectively reseting the flow with fresh fuel before the detonation returns. The detonation front always interacts with a fresh fuel mixture, and the reacting flow is confined by hot product gases from previous cycles.

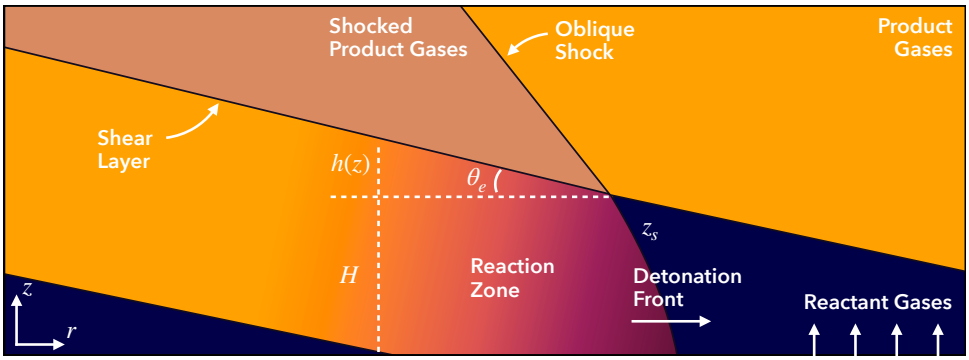

Figure 1: Continuous detonation engine schematic for a planar configuration with periodic boundary conditions at left and right, an outflow boundary at the top, and a fuel inflow boundary at the bottom.

The resulting system maintains a stable detonation that operates at an effective channel height H with a shear layer at an effective deflection angle θ_e. The effective channel height depends on the length of the channel and the mass flow rate of the fuel. The shear layer deflection angle that forms between the detonating mixture and detonation product gases depends on the reacting/product gas impedance ratios [2]. This deflection induces flow divergence in the reacting flow, which in turn leads to curvature along the detonation front.

The aim of this work is to directly assess how the channel height and deflection angle of the shear layer affect detonation performance for a simplified one-step reaction mechanism. Using a shock-fitted flow formulation [3], both parameters are independently controlled. This in turn allows us to define size effect and detonation front shape characteristics, and subsequently calibrate a detonation shock

Correspondence to: svoelkel@lanl.gov

dynamics (DSD) model. The resulting DSD model is then shown to accurately predict performance data for a wide range of channel configurations.

2 Governing Equations

For this work, 2D planar detonations are analyzed via the non-dimensional Euler equations with one-step reaction kinetics:

$$\frac{\partial}{\partial t}\begin{bmatrix}\rho\\ \rho u_r\\ \rho u_z\\ \rho E\\ \rho\lambda\end{bmatrix}+\frac{\partial}{\partial r}\begin{bmatrix}\rho u_r\\ \rho u_r^2+p\\ \rho u_r u_z\\ u_r(\rho E+p)\\ \rho u_r\lambda\end{bmatrix}+\frac{\partial}{\partial z}\begin{bmatrix}\rho u_z\\ \rho u_r u_z\\ \rho u_z^2+p\\ u_z(\rho E+p)\\ \rho u_z\lambda\end{bmatrix}=\begin{bmatrix}0\\ 0\\ 0\\ 0\\ \rho\Lambda\end{bmatrix}, \tag{1}$$

where ρ is the density, u_r and u_z are the velocity components in the r and z directions, respectively, p is the pressure, $E = e + \left(u_r^2 + u_z^2\right)/2$, where e is the internal energy, and λ is the reaction progress variable, which is bounded between zero and one for an unreacted and fully reacted mixture, respectively. These properties are normalized by the ambient pressure and density, and the length scale is set so that the half-reaction length of the ZND wave is one [4]. An ideal gas model and a one-step Arrhenius reaction mechanism are employed to close the system and are given by

$$e = \frac{p}{\rho(\gamma-1)} - q\lambda, \quad T = \frac{p}{\rho}, \quad \Lambda = k(1-\lambda)e^{-E_a/T}, \tag{2}$$

where γ is the ratio of specific heats, q is the heat release, T is the temperature, k is the rate constant, and E_a is the activation energy. Here, we set $\gamma = 1.2$, $q = 50$, which results in Chapman-Jouguet velocity $D_{CJ} \approx 6.8095$, $E_a = 15$, and $k \approx 7.6648$, which results in our desired length scale so that for a ZND profile, $x = 1$ when $\lambda = 0.5$.

This system of equations is solved using shock-fitted formulation [3], wherein the denotation front is treated as a boundary condition of the flow. Front surface evolution equations for D_n and $\partial z_s/\partial r$ are solved in tandem with the reactive Euler equations. Furthermore, the shear layer interface is approximated as a straight streamline boundary at a given deflection angle. The equations in the physical space as defined in Eq. (1) are transformed onto a Cartesian $\xi - \eta$ frame via the following relations:

$$r = \xi\left(1 + f(\tau)\cdot h(\eta)/H\right), \quad z = z_s(\xi,\tau) + \eta, \quad t = \tau, \tag{3}$$

where $h(\eta) = \tan^{-1}\theta_e \cdot \eta$ defines the streamline deflection, and $f(\tau)$ is a function that ramps from zero to one over time (see [3]). The validity of this shock-fitted formulation, specifically the use of a streamline boundary condition to represent the shear layer, has been previously demonstrated by comparing divergent shock-fitted and corresponding multi-material simulations [4].

With the shock-fitted formulation, the system is now numerically solved in $\xi - \eta$ frame via standard finite volume methods. For this work, we set the resolution to have 20 points in the half-reaction-zone. A centered MinMod flux is limiter employed for interior cells, except at detonation shock front, where flux is set directly based on the local shock state. Finally, D_n along the front is evolved by extrapolating the interior flow to the shock front surface. Further formulation and numerical details on this implementation can be found in [3].

3 Simulation Results

Each simulation is initiated via a ZND solution in channel configuration, i.e. with $\theta_e = 0°$. After initializing the flow, the streamline is ramped up to a desired deflection angle, after which the detonation experiences a transient period before developing a stable flow. Figure 2 shows the standard features observed for each of simulations performed in this work. Initially, the flow is a steady ZND solution.

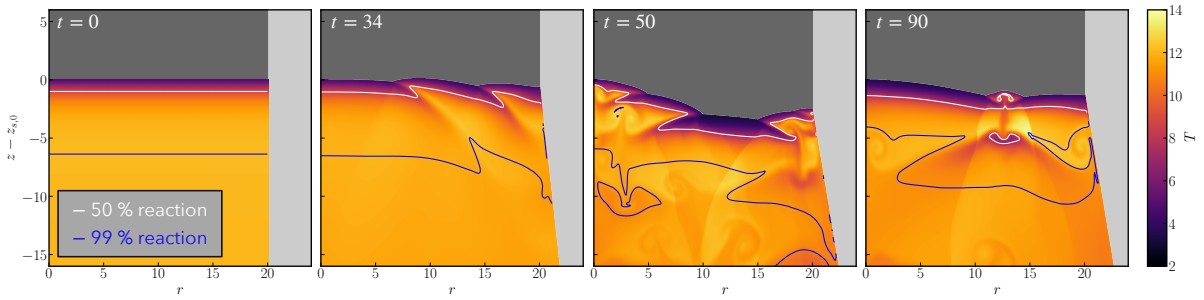

Figure 2: Simulation snapshots for $H = 20$ and $\theta_e = 10°$

Between $t = 10-50$, the streamline deflection angle is increased until the desired θ_e is obtained. During this time, weak transverse waves initiated at the streamline move towards the axis of symmetry. These transverse waves grow in strength as they reflect at the axis of symmetry and subsequently interact with additional incoming waves. These waves continue to reflect between the axis of symmetry and the streamline, growing until eventually developing into a cellular structure. Finally, the flow relaxes towards a stable (consistent) cellular detonation structure based on the deflection and channel height.

Time-averaged data was extracted from each of the simulations after the flow relaxed to a stable cellular detonation structure. For each configuration tested, the detonations were observed to be stable beyond time 200. Between time 200 and 300, 1000 snapshots of the front shape were recorded. These snapshots were in turn used to define the time-averaged front shape, as shown in Fig. 3. Though the front shape

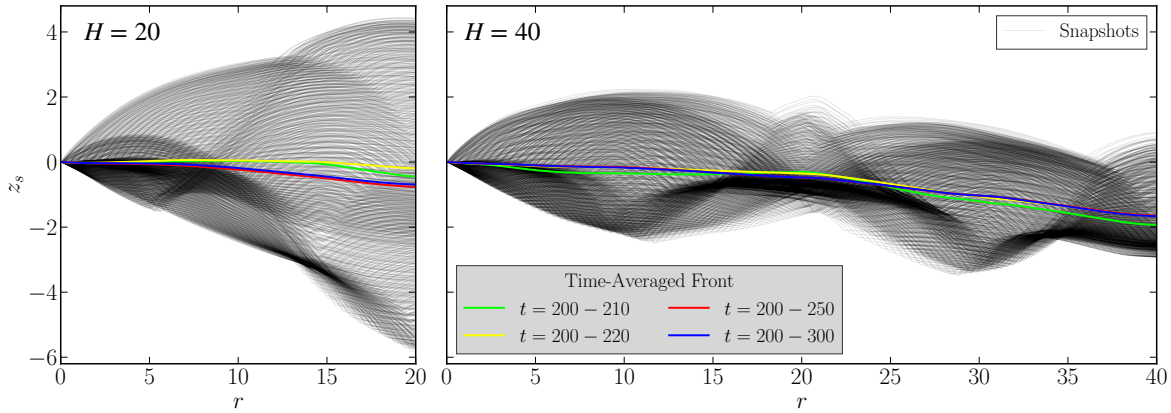

Figure 3: Front shape snapshots at $\theta_e = 10°$ for varied charge sizes between time 200 and 300, as well as time-averaged front-shapes over various time ranges.

varies significantly throughout this time period due to the cellular instability, the resulting time-averaged front shapes are surprisingly smooth. In addition to the time-averaged front shape, the time-averaged detonation velocity D_0 was calculated based on the distance the detonation traveled in the lab frame from time 200 to 300.

4 Cellular Detonation Dynamics Analysis

To quantify the detonation dynamics, a series of simulations were performed with θ_e varied between $0°$ and $20°$, and H varied between 4 and 80. For each simulation, the time-averaged phase velocity and front shapes were extracted using the previously described methodology. The results are shown in Fig. 4. At zero degrees, we observe similar results for all channel heights, with D_0 slightly greater

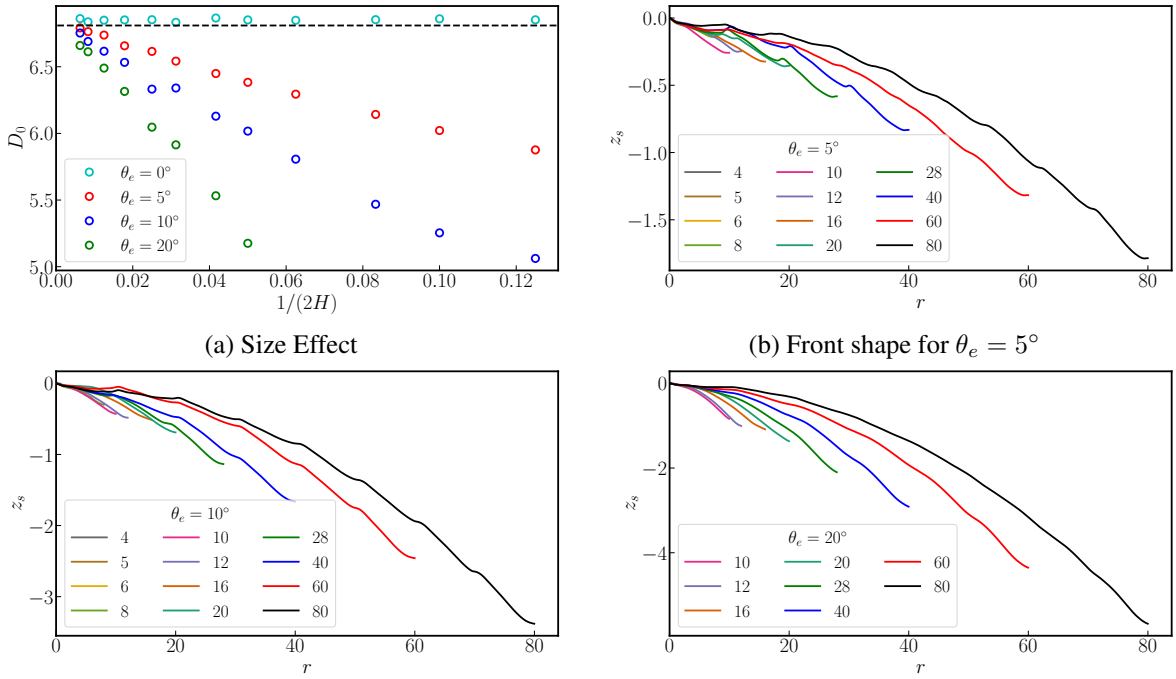

(a) Size Effect

(b) Front shape for $\theta_e = 5°$

(c) Front shape for $\theta_e = 10°$

(d) Front shape for $\theta_e = 20°$

Figure 4: Time-averaged performance data for a range of edge angles and charge sizes.

than D_{CJ}. For deflection angles greater than zero, we observe typical size effect behavior, namely that the detonation velocity increases as the charge size increases, approaching D_{CJ} for large channel heights. The size effect curves are not completely smooth though, likely an effect of the flow becoming mode-locked to maintain a specific number of cells.

The time-averaged front shapes are approximately smooth from the axis towards the sidewall and show an underlying curvature effect at each deflection angle and channel height. The averaged curvature effects are more dominant compared to the cellular structures at larger channel heights. For lower deflection angles, and for smaller charge sizes, the deflection and subsequent curvature is likely not the leading factor in determining the global behavior compared to the cellular instability.

The simulated detonation performance data is modeled for predictive applications via Detonation Shock Dynamics (DSD), wherein the detonation shock and reaction zone are modeled as a single surface evolution equation. This formulation is motivated by asymptotic analysis assuming local curvature is small compared to the inverse of a characteristic reaction zone length. The resulting surface evolution equation is governed by a level set dependent on normal velocity D_n, which itself is a model function dependent on the local curvature along the detonation front κ. The detonation front shape is determined by set a of ODEs dependent on ϕ (the angle between the normal surface direction and the axial direction), integrated between 0 and ϕ_e (the edge angle). The ODEs for planar geometries and our choice for a

$D_n - \kappa$ relation are given by

$$\frac{dr_s}{d\phi} = \frac{\cos\phi}{\kappa}, \quad \frac{dz_s}{d\phi} = -\frac{\sin\phi}{\kappa}, \quad \cos\phi = \frac{D_n}{D_0}, \quad D_n(\kappa) = D'_{CJ}\left[1 - \frac{B\kappa}{1 + C_4\kappa}\right]. \tag{4}$$

We found that both simplified and more complex $D_n - \kappa$ forms did not improve the calibration results.

The DSD model was calibrated for the series of simulations at $\theta_e = 10°$. The model parameters B, C_4 and ϕ_e were simultaneously calibrated via standard minimization techniques using a Nelder-Mead method to minimize a merit function based on the size effect and front shape data [5]. D'_{CJ} was set to 6.85 to match channel flow simulation results. The resulting calibration yielded model parameter values of $B = 15.00$, $C_4 = 11.34$, and $\phi_e = 5.089$.

The calibration results are shown in Fig. 5. In general, the DSD model accurately reproduces both the size effect and front shape data. The errors among size effect points are evenly spread, and the largest

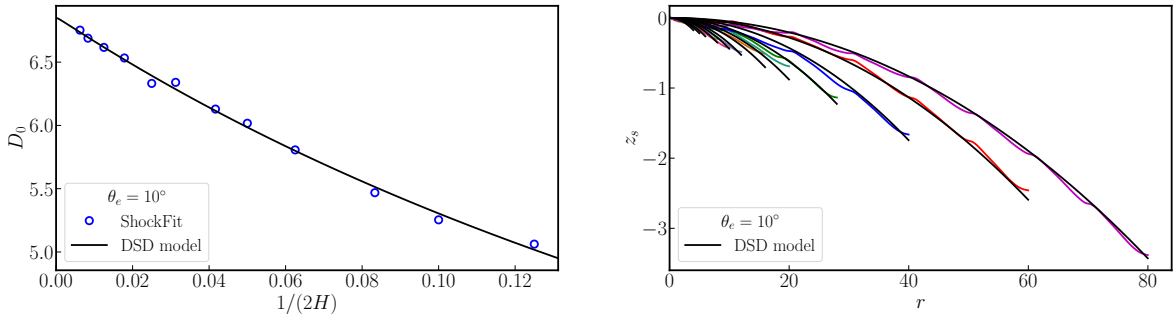

(a) Size Effect (b) Front shape

Figure 5: DSD calibration results for $\theta_e = 10°$.

front shapes are most accurately reproduced. Again, we note that the smaller channels sizes may not be well-suited for DSD modeling as the curvature is likely not be the leading factor in determining the global behavior, which may inhibit DSD's modeling capability.

The DSD model as calibrated for $\theta_e = 10°$ was then used to predict the performance at varied deflection angles. For each deflection angle, the same D'_{CJ}, B, and C_4 values are used, but the edge angle ϕ_e must be modified to be consistent with the selected deflection angle θ_e. We assign ϕ_e for a given θ_e by optimizing the corresponding front shape at $H = 20$, which gives $\phi_e = 2.579°$ for $\theta_e = 5°$ and $\phi_e = 8.925°$ for $\theta_e = 20°$. The model was then used to predict the corresponding detonation size effect and front shapes at varied sizes for each deflection angle.

The DSD model predictions for $\theta_e = 5°$ and $20°$ are shown in Fig. 6. Overall, the DSD model accurately predicts the size effect and front shape data for each of the deflections angles. The large channels are predicted most accurately, whereas for small channels, the flow is dominated by cellular evolution. At larger deflection angles, the DSD models does a remarkably good job matching the time-averaged front shape and size effect data, suggesting that the streamline deflection and subsequent curvature along the front are the leading factors driving the performance characteristics. This is in spite of the flow maintaining a cellular detonation structure. For such configurations, the DSD model presents a viable strategy for predicting average detonation characteristics for a wide range of configurations.

5 Conclusions

In this work, channel height and streamline deflection in planar detonations were analyzed via 2D shock-fitted formulation. An ideal gas and one-step Arrhenius model were employed. We showed time-

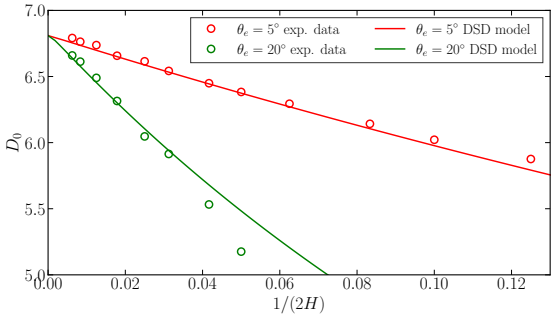

(a) Size Effect

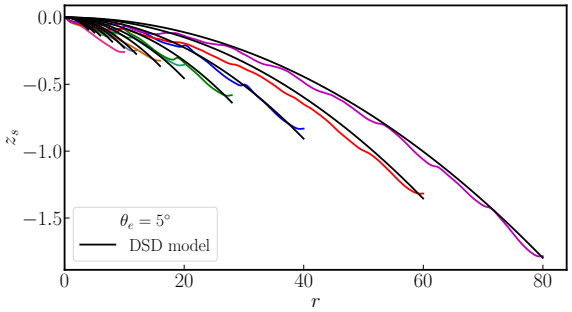

(b) Front shape for $\theta_e = 5°$

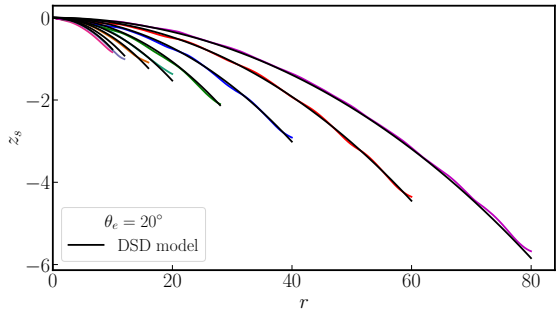

(c) Front shape for $\theta_e = 20°$

Figure 6: DSD model predictions for $\theta_e = 5°$ and $\theta_e = 20°$.

averaged size effect and front-shape data for a wide range of heights and deflection angles. A DSD model was calibrated at a fixed a deflection angle, and the resulting model accurately represented the time-averaged data. This model was then shown to accurately predict size effect and front shapes at both greater and lesser deflection angles.

References

[1] V. Raman, S. Prakash, and M. Gamba, "Nonidealities in rotating detonation engines," *Annual Review of Fluid Mechanics*, vol. 55, 2023.

[2] W. P. Sommers and R. B. Morrison, "Simulation of condensed-explosive detonation phenomena with gases," *The Physics of Fluids*, vol. 5, no. 2, pp. 241–248, 1962.

[3] C. Chiquete, M. Short, C. D. Meyer, and J. J. Quirk, "Calibration of the pseudo-reaction-zone model for detonation wave propagation," *Combustion Theory and Modelling*, vol. 22, no. 4, pp. 744–776, 2018.

[4] C. Chiquete, M. Short, and J. J. Quirk, "The effect of curvature and confinement on gas-phase detonation cellular stability," *Proceedings of the Combustion Institute*, vol. 37, no. 3, pp. 3565–3573, 2019.

[5] S. J. Voelkel, E. K. Anderson, M. Short, C. Chiquete, and S. I. Jackson, "Effect of lot microstructure variations on detonation performance of the triaminotrinitrobenzene TATB-based insensitive high explosive PBX 9502," *Combustion and Flame*, vol. 246, p. 112373, 2022.